Rutile Growth Mechanism on TiC Monocrystals by Oxidation

A. Bellucci and D. Gozzi*

Dipartimento di Chimica, Università di Roma "La Sapienza", P.le Aldo Moro 5, 00185 Roma, Italy

M. Nardone and A. Sodo

Dipartimento di Fisica, Università dell'Aquila, Via Vetoio, Coppito, l'Aquila, Italy

Received May 21, 2002. Revised Manuscript Received December 13, 2002

The surfaces (111) and (110) of TiC single crystals have been exposed to an Ar/O_2 mixture at low oxygen content (≈270 ppm, $P_{tot} = 2$ bar abs.) and 1073 K. The oxygen consumption and interaction gaseous products have been detected, respectively, through zirconia stabilized oxygen sensors and a quadrupole mass spectrometer. The cross-sections of oxidized samples have been analyzed by micro-Raman and SEM techniques. Concentration profiles of amorphous carbon and rutile have been detected along the carbide oxidized layer interface. This confirms previous observations of retention of carbon during the oxidation of the transition metal carbides. The results obtained have been compared with our previous experiments which showed the following structural relationships: $TiO_2(200)||TiC(111)$ and $TiO_2(110)||TiC(110)$. The rutile (200) growth rate was found to be higher than the growth rate of rutile (110). Oxidation routes have been proposed.

1. Introduction

Transition metal carbides are high-temperature materials having physicochemical characteristics typical of ceramics and electronic properties resembling metals, and they have challenged a lot of investigations.[1−6] They are interesting from a theoretical as well as technological point of view as several applications of them are apparent. They have traditionally been used under extreme conditions of temperature and pressure, so that extensive oxidation studies of transition metal carbides in general, and in particular TiC,[6−10] have been undertaken by many authors. By using gas mixtures very dilute in oxygen[11,12] we can analyze the early stages of oxidation in order to identify the mechanism which allows the carbide structure to turn into the structure of the oxidation product. Literature data referring to this particular condition are very few and often scattered.

The present paper reports the results obtained by investigating TiC interaction with oxygen at low partial pressure (≈27 Pa) and high temperature (1073 K). The (111) and (110) faces of TiC single crystals have been studied. The knowledge of the interaction mechanism is fundamental to foresee the modifications of the growing interface (carbide/oxidation product) as well as the way of driving the gas−solid reaction to design a final carbide/oxide interface having the required properties. Though the mechanical properties of transition metal carbides are very good in terms of hardness especially, those properties can be destroyed in air and at high temperature because the chemical stability is poor. A compact adherent oxide layer, previously grown upon the carbide surface, could be protective and suitable to hold the mechanical properties in such conditions. Scope of the present work is to contribute to establishing the growth mechanism of parent oxide films upon refractory carbides.

2. Experimental Section

Apparatus. The experimental apparatus used in our laboratory consists of a homemade device based on two identical solid electrolyte oxygen sensors, S_r and S_m, connected to a quadrupole mass spectrometer (QMS). In both the sensors the electrolyte is a round tube closed at one end and made of 8 mol % yttria stabilized zirconia. All the details are given in the literature.[11−15] The basic operation principle is the measure of the reaction rate, r, as the change between the inlet oxygen

* Corresponding author. E-mail: Daniele.Gozzi@uniroma1.it.

(1) Johansson, L. I. *Surf. Sci. Rep.* **1995**, *21*, 177.
(2) Williams, W. S. *Mater. Sci. Eng.* **1998**, *A105/106*, 1.
(3) Oyama, S. T. In *The Chemistry of Transition Metal Carbides and Nitrides*, Oyama, S. T., Ed.; Blackie Academic & Professional: Glasgow, Scotland, 1996; Chapter 1.
(4) Lei, J.-F.; Okimura, H.; Brittain, J. O. *Mater. Sci. Eng.* **1990**, *A123*, 129.
(5) Williams, W. S. *JOM* **1997**, *49*, 38.
(6) Storms, E. K. *The Refractory Carbides*; Academic Press: New York, 1967.
(7) Stewart, R. W.; Cutler, I. B. *J. Am. Ceram. Soc.* **1967**, *50*, 4.
(8) MacDonald, N. F.; Ransley, C. E. *Powder Met.* **1959**, *3*, 172.
(9) Webb, W. W.; Norton, J. T.; Wagner, C. *J. Electrochem. Soc.* **1956**, *103*, 112.
(10) Shimada, S.; Yunazar, F.; Otani, S. *J. Am. Ceram. Soc.* **2000**, *83*, 721.
(11) Gozzi, D.; Cascino, G.; Loreti, S.; Minarini, C.; Shimada, S. *J. Electrochem. Soc.* **2001**, *148*, J15.
(12) Bellucci, A.; Di Pascasio, F.; Gozzi, D.; Loreti, S.; Minarini, C. *Thin Solid Films* **2002**, *405*, 1.
(13) Gozzi, D.; Guzzardi, G.; Montozzi, M.; Cignini, P. L. *Solid State Ionics* **1997**, *101−103*, 1243.

10.1021/cm021204c CCC: $25.00
Published on Web 02/14/2003

flux in the reaction chamber and the outlet oxygen flux from it: $r = J(x_{in} - x_{out})$, where J is the flow rate of the gas mixture and x_{in} and x_{out} are, respectively, the oxygen molar fraction in the inlet and outlet flux. The reaction chamber is inside a furnace where any thermal cycle, up to a maximum temperature of 1273 K, can be performed. Close to the sample an S-type thermocouple measures the actual temperature. Mixtures with any oxygen content can be prepared by operating mass flow controllers. They mix the carrier gas, high purity Ar, with an Ar/O_2 mixture whose oxygen content is fixed and known. One of the two sensors, S_r, detects x_{in}. According to the Wagner equation, the electromotive force (emf, E) of the sensors is given by $E = {}^1/_4 \int_{\mu O_2^o}^{\mu O_2^i} t_{v_O} d\mu_{O_2}$. The terms $\mu^o_{O_2}$ and $\mu^i_{O_2}$ are, respectively, the oxygen chemical potential at the outer and inner side of the electrolyte tube, and t_{v_O} is the transport number of the oxygen vacancies. Both the oxygen sensors operate in the electrolyte domain of the stabilized zirconia, i.e., t_{v_O} is close to 1. In the outer side of S_r, pure oxygen flows as reference. Before entering the reaction chamber the gaseous mixture passes first in the inner side of S_r and then in the inner side of the other oxygen sensor, S_m. After having reacted with the sample in the reaction chamber, the gaseous stream circulates in the outer side of S_m. By assuming for the gaseous species an ideal behavior, we can calculate the reaction rate, r, according to the following equation:

$$r = J(x_{in} - x_{out}) = J \exp[(E_m - E^*_m)/AT_m]\{1 - \exp[(E^*_r - E_r)/AT_r]\} \quad (1)$$

where E_m and E_r are the E values given respectively by the oxygen sensors S_m and S_r; E^*_m and E^*_r are experimentally determined constants; A is ${}^R/_{4F}$ with R = gas constant and F = Faraday constant; T_m and T_r are, respectively, the temperatures of S_m and S_r determined by S thermocouples. By integrating eq 1 it is possible to calculate the total amount of oxygen consumed by the sample in a given time interval. The outlet of S_r is connected to a QMS by a stainless steel capillary 1 m long with a 150-μm i.d. The pressure gradient at its ends is kept constant in such a way as to maintain a constant viscous flow. The pressure at QMS inlet is kept at 1 mbar by a vacuum rough pump. The injection of the gas mixture into the QMS chamber is regulated fine by a dosing valve (Balzers). Mass spectrometric measurements have been performed routinely in multiple ion detection (MID) mode through the PC-QMS data acquisition system. The energy of the electron beam was set at 70 eV and at this value the ionization probability ratio between CO_2 and O_2 has been found to be 1.4.

The Raman spectra have been collected using a Labram spectrometer by Dilor. The excitation source has been an Ar^+ ion laser ($\lambda = 514.5$ nm). The illumination and collecting optics of the system consists of a microscope in confocal configuration. The quality of the laser beam and the use of a confocal microscope allow us to obtain a spatial resolution less than 3 μm. The motion scans were performed using a piezo-electric transducer scanning a range of 50 μm in 1-μm steps. The spectrometer achieves the high contrast required for the rejection of the elastically scattered component by coupling appropriate optical notch filters to a grating monochromator. A high counting efficiency of the system is guaranteed by a cooled 1024 × 256 pixel CCD detector. The dimensions of the pixels (about 24 μm) determine the ultimate resolution of the instrument, which turns out to be on the order of ± 1 cm^{-1}. The laser power irradiated on the sample was 10 mW.

Samples. The TiC single crystals have been cut from raw crystals prepared by a floating zone technique. They appear to be C free as found by the micro-Raman analysis where no signal was detected in the whole wavenumber range from 58 to 1750 cm^{-1} as reported also in the literature.[16] They have been fully coated by gold sputtering except for one surface that is the side exposed to the gaseous mixture. The thickness of the gold coating is ~1 μm and the quality of covering the TiC substrate was checked by SEM microprobe analysis by repeating the sputtering until the Ti signal disappeared. Pieces almost square and uniform in thickness, (0.71 ± 0.01) and (1.26 ± 0.01) mm, respectively, for the samples with exposed surfaces (111) and (110), have been used. The exposure of only one side of the sample simplifies the analysis of the species profiles along the sample cross-section. The exposed surface areas were (7.60 ± 0.01) mm^2 for both the samples. The oxygen partial pressure value was set at (27.1 ± 0.1) and (28.0 ± 0.1) Pa, respectively, for TiC(111) and TiC(110). Thermal cycles were constituted by two symmetrical heating and cooling ramps (|10| K min^{-1}) and an 8-h isotherm. The isotherm temperatures were (1073 ± 1) K for TiC(111) and (1075 ± 1) K for TiC(110).

The weight of the samples was on the order of a few tenths of milligrams: (26.83 ± 0.01) and (47.17 ± 0.01) mg respectively for TiC(111) and TiC(110).

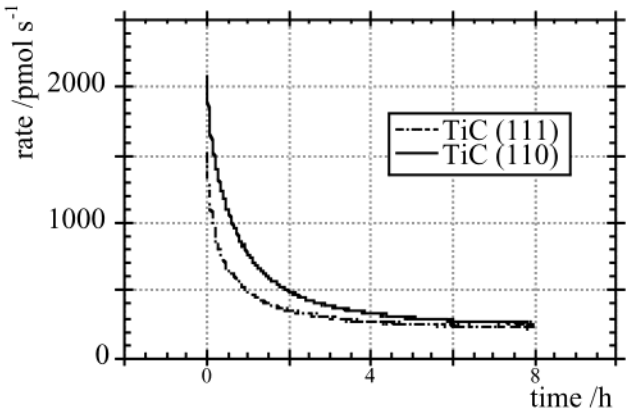

Figure 1. Oxygen consumption rate calculated by eq 1 through the emf values of the solid electrolyte oxygen sensors. Time interval is equal to the length of the isotherms at (1073 ± 1) K, TiC (111), and (1075 ± 1) K, TiC (110).

3. Results

The reactivity of the samples, given as oxygen consumption rate, is reported in Figure 1. It refers to the surfaces (111), dashed line, and (110), solid line, of two single crystals. The value of the reactivity has been calculated, according to eq 1, along the isotherm. The trend of the reactivity is always decreasing without approaching zero in the time interval of the isotherm. Figure 2 shows the QMS signals displayed as difference between the ionic current values at room temperature, where no reactivity of the sample exists, and at time t during the isotherm: negative values of ΔI mean consumption, positive values of ΔI mean production of the gaseous species considered. By using the difference, the QMS chamber background is practically removed from the detected ionic currents. The ΔI error bars should be considered within 0.5% of the value. As shown by Figure 2, we have detected for both the samples the O_2 consumption, as given by the oxygen sensors too (Figure 1), and CO_2 production; no CO evolution during the isotherm has ever been detected in the present experiments. The ratio $\Psi = |\Delta I_{CO_2}/\Delta I_{O_2}|$, reported in the right ordinate of Figure 2, is a measure at each time t

(14) Gozzi, D.; Cignini, P. L.; Montozzi, M. In *High-Temperature Materials Chemistry IX*; Spear, K. E., Ed.; The Electrochemical Society: Pennington, NJ, 1997; Vol. 97-39, p 787.

(15) Gozzi, D.; Guzzardi, G.; Salleo, A. *Solid State Ionics* **1996**, *83*, 177.

(16) Yajima, F.; Tanka, T.; Bannai, E.; Kawai, S. *J. Crystal Growth* **1979**, *47*, 493.

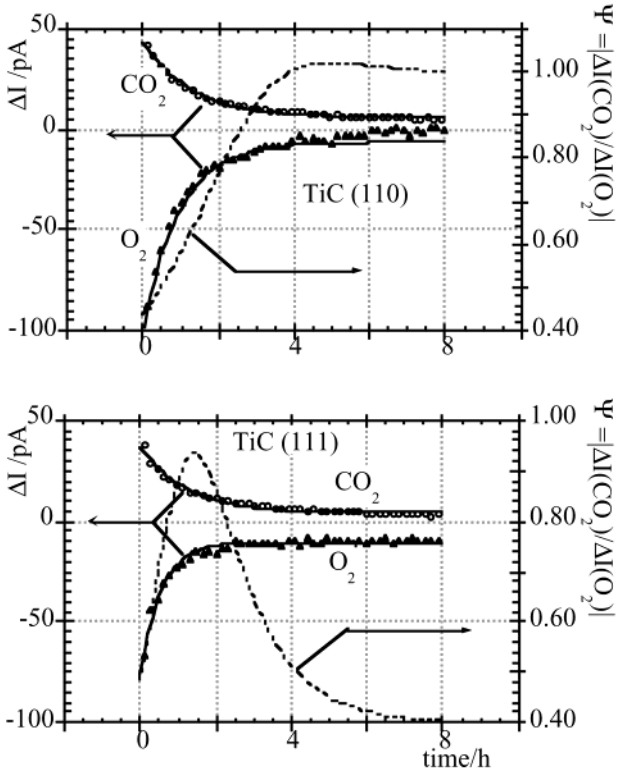

Figure 2. Top: TiC(110). Left ordinates: QMS signals of O_2 and CO_2 and best-fitting curves $\{\Delta I(O_2) = -6.14 - 93.6 \exp(-1.036t)$; $\Delta I(CO_2) = 6.10 + 37.4\exp(-0.794t)\}$. Right ordinates: quantity Ψ given by the ratio $|\Delta I(CO_2)/\Delta I(O_2)|$. Time interval is equal to the length of the isotherms. Bottom: TiC-(111). Left ordinates: QMS signals of O_2 and CO_2 and best-fitting curves $\{\Delta I(O_2) = -10.48 - 65.8 \exp(-1.830t)$; $\Delta I(CO_2) = 4.19 + 32.9\exp(-0.825t)\}$. Right ordinates: quantity Ψ given by the ratio $|\Delta I(CO_2)/\Delta I(O_2)|$. Time interval is equal to the length of the isotherms.

of the weight of the combustion of carbon with respect to the oxidation reactions of TiC. The quantity Ψ has been obtained as the ratio of the best fitting equations of the experimental curves ΔI vs t assuming that the proportionality factor between ΔI and partial pressure in the QMS chamber of both CO_2 and O_2 species is the same. The range of Ψ is $0 \leq \Psi \leq 1$ where the limits represent, respectively, the complete embedding of oxygen in the condensed phase without any production of CO_2 and complete combustion of carbon as unique process.

Micro-Raman spectra of the oxidized samples have been obtained by scanning the cross-section perpendicularly to the direction of the laser beam, from the bulk of the sample toward the surface exposed to the gaseous mixture (Figure 3). At each 1-μm step, a spectrum has been recorded. The micro-Raman analysis has been performed three times per each sample, any time starting from a different point of the bulk of TiC and scanning a displacement range of 50 μm. Three similar profiles have been obtained for both the samples. For the sake of clarity, we show only one profile per sample and only those scans that detected Raman signals. In fact, because of the NaCl structure, Raman spectra are not detectable from the unreacted areas of the TiC samples. The absence of any Raman signal from the bulk of the samples confirms also that the samples were C free, as expected. The analysis of the Raman spectra detected in the outer region of the sample, which

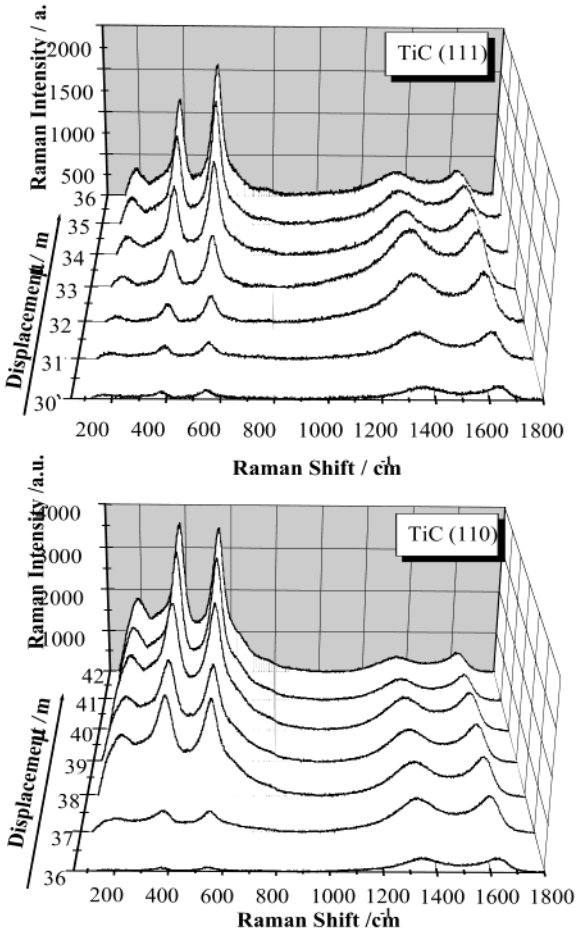

Figure 3. Micro-Raman spectra along the cross-section of the reacted region (rutile, peaks at 249, 446, and 613 cm^{-1}; amorphous carbon, peaks at 1377 and 1605 cm^{-1}). The origin of the displacement axis is in an arbitrary point in the bulk of TiC where no micro-Raman signal is detected. Lower scan numbers refer to the TiC/reacted region. Higher scan numbers refer to reacted region/gas interface.

reacted with the gaseous mixture, revealed the presence of five peaks. The features appearing at 249, 446, and 613 cm^{-1} should be attributed to rutile.[17,18] The Raman modes involve only the movement of oxygen ions and corresponding stretching and bending of the Ti−O anchored in place. The doublet located around 1377 and 1605 cm^{-1} reveals the presence of amorphous carbon.[19,20] The two features are named respectively G and D peaks. Raman spectroscopy offers a powerful method for identifying carbon as one can determine its crystallographic arrangement. From graphite to amorphous carbon, the G peak broadens and becomes less intense while the D peak appears gradually. In the present case, considering the characteristic shape and position of both the peaks, they have been assigned to amorphous carbon, also in agreement with literature.[19,20]

Carbon observed has to be produced by the gas−solid reaction, and the coexistence of amorphous carbon and rutile in the reacted region upon the TiC substrate is

(17) Betsch, R. J.; Park, H. L.; White W. B. *Mater. Res. Bull.* **1991**, *26*, 613.
(18) Turkovic, A.; Ivanda, M.; Drasner, A.; Vranesa, V.; Persin, M. *Thin Solid Film* **1991**, *198*, 199.
(19) Sze, S. K.; Siddique, N.; Sloan, J. J.; Escribano, R. *Atmos. Environ.* **2000**, *35*, 561.
(20) Huong, P. V. *Mater. Sci. Eng.* **1992**, *B11*, 235.

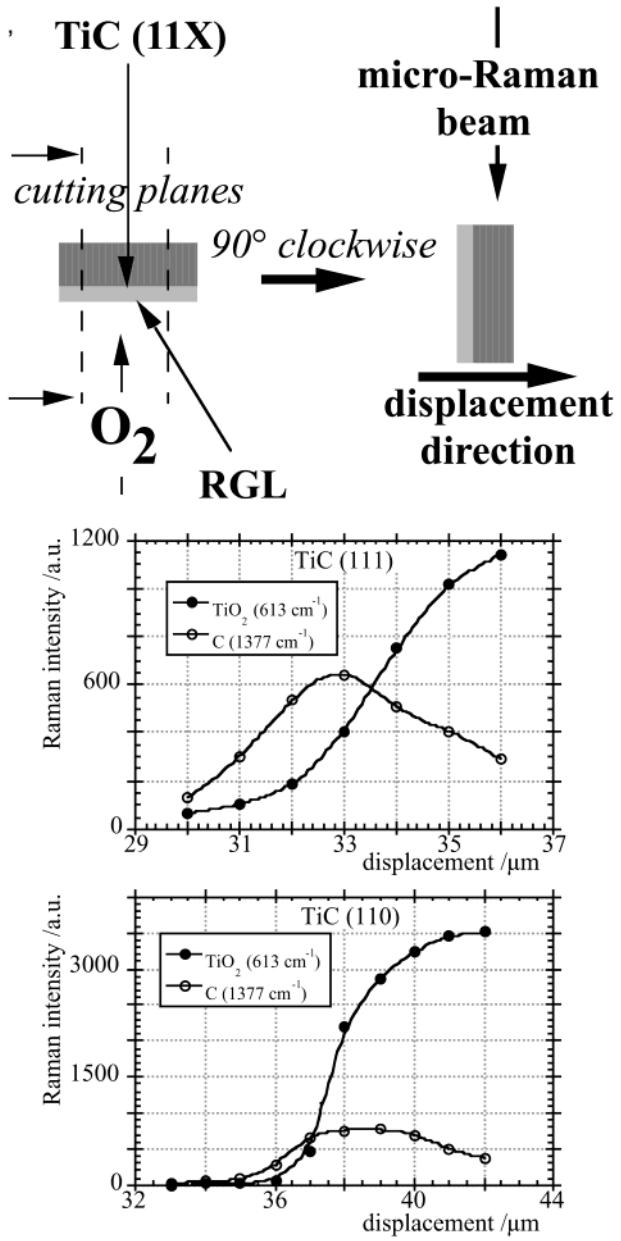

Figure 4. Micro-Raman intensity profiles of rutile and amorphous carbon taken at their most intense peaks, respectively, at 613 and 1377 cm^{-1} as a function of the displacement along the cross-section of the reacted region. The origin of the displacement axis is in an arbitrary point in the bulk of TiC where no micro-Raman signal is detected. Lower scan numbers refer to the TiC/ reacted region interface. Higher scan numbers refer to reacted region/gas interface. The uppermost figure is a scheme showing the position of the sample during the oxidation and the position of its cross-section in the micro-Raman profile analysis.

clearly shown. The detection of the rutile agrees with our previous results obtained in similar experimental conditions[11,12] where XRD analysis and XRD texture revealed an oriented growth of a TiO_2 layer on the TiC single crystal substrate. The intensities of both the C and rutile micro-Raman signals are not constant throughout the cross section. To simplify the analysis of the profiles, only the trend of the most intense peak, respectively, for C (1360 cm^{-1}) and rutile (610 cm^{-1}), has been considered and reported in Figure 4. In the same figure, the uppermost panel shows the position of the sample during the oxidation and the position of its

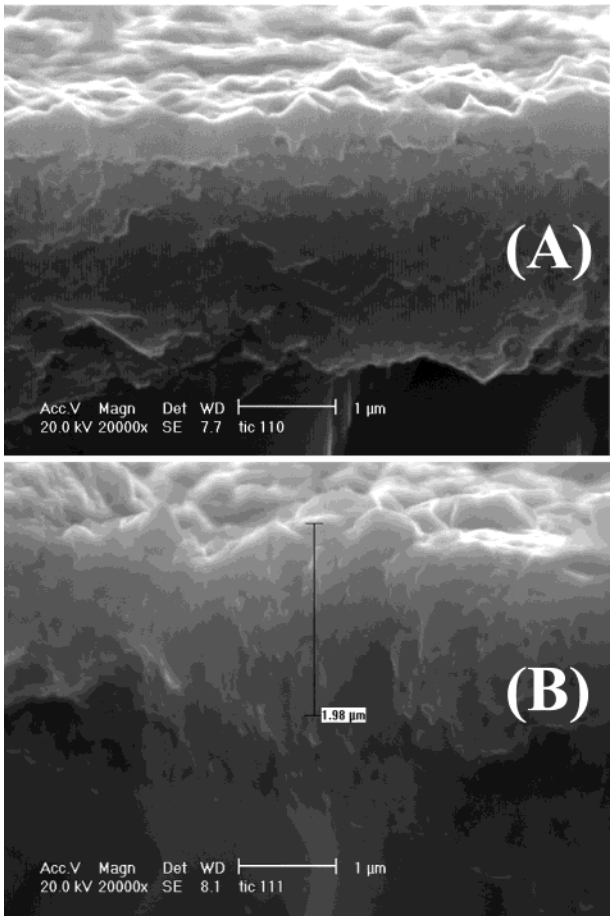

Figure 5. Morphology by SEM of the cross-section of the oxidized samples. In both photographs the lighter layers are attributed to rutile. The darker layers below are attributed to the region which reacted partially. A: TiC (110), upper photograph; B: TiC (111), lower photograph.

cross-section in the micro-Raman analysis. Moving from the inner (lower scan numbers) region, close to the TiC substrate, outward (higher scan numbers), the intensity of the rutile signal increases, whereas the intensity of C reaches a maximum and then decreases.

SEM analysis of the cross section of the oxidized samples (Figure 5) showed a compact layer grown on the TiC substrate for both the samples.

4. Discussion

According to the micro-Raman profiles (Figures 3 and 4), and CO_2 production and O_2 consumption rates (Figure 2), the oxidation mechanism of transition metal carbides can be better understood with respect to the present scenario as given in the literature.[10−12] Before starting the discussion, it is important to point out that we are dealing with two different sets of experimental evidence: real time data concerning the kinetics of the O_2 consumption and CO_2 production in isothermal conditions; and micro-Raman analyses which are "pictures" of the carbide/oxide interface at the end of the isotherm, taken at room temperature − without considering, for the sake of simplicity, the effect of cooling, if any. A further consideration to take into account is what occurs during the heating of the sample from room temperature up to the isotherm. It is evident that oxide is already present at the beginning of the isotherm.

The main working hypothesis is that the rutile growing layer, RGL, is a compact layer within which the solid-state transport of oxygen occurs. If so, a chemical potential gradient of oxygen vacancies, $V_{\ddot{O}}$, should be established at RGL interfaces in such a way as to allow the diffusion−migration of them from the rutile/carbide to gas/rutile interface while a flux of oxygen atoms moves in the opposite direction. Similarly to the model of the parabolic oxidation of metals, the driving force of the process is the gradient of the oxygen chemical potential at RGL interfaces, and the rate-limiting step of the process is the solid-state transport within RGL. Throughout this paper, the Kröger and Vink notation will be adopted. At the rutile/carbide interface, oxygen reacts with the carbide phase according to the reaction of point defects:

$$C_C + O_O = O_C^x + C_i^x + V_{\ddot{O}} + 2e' \quad (2)$$

or, more usually, in the case of TiC

$$TiC + yO = TiC_{1-y}O_y + yC \quad (3)$$

where the oxygen goes into the site of carbon, O_C, producing an oxygen vacancy, and carbon is displaced in interstitial position, C_i^x. This is equivalent to the formation of a new phase adjoining the RGL, the chemical nature of which corresponds to the composition of a Ti-oxycarbide. Any further increase of oxygen above a certain value of the ratio $y/(1 - y)$ produces the transformation into rutile as given by reaction

$$TiC_{1-y}O_y + \epsilon O = \beta TiO_{2-x}(\gamma C) + \delta TiC_{1-y'}O_y \quad (4)$$

where $y' > y$, $(\beta + \delta) = 1$, $\gamma = [(1 - y) - \delta(1 - y')]/\beta$, and $\epsilon = y(\delta - 1) + \beta(2 - x)$.

This means further growth of the RGL and each new rutile thin layer dissolves carbon according to the thermodynamics of reaction 4. Thus, a chemical potential gradient of C, $\nabla\mu_C$, exists which is oriented toward the rutile/gas interface where carbon diffuses to be burnt as CO_2. It is reasonable to assume that the condition of the maximum value of $\nabla\mu_C$ is always fulfilled because the carbon activity at the rutile/gas interface is zero due to the rapid consumption of carbon sustained by the combustion reaction. At the location where reaction 4 occurs, the activity of carbon in rutile should be proportional to the solid solubility of carbon in rutile at the isotherm temperature. Therefore, $\nabla\mu_C$ decreases with time together with the carbon flux within the RGL because the oxide thickness increases in time. This implies that the boundary conditions of the carbon diffusion change continuously due to the displacement of the carbon source.

The proposed mechanism is sketched in Figure 6 where a moving boundary of a given thickness displaces from rutile to carbide, forming rutile at its right side and consuming carbide at its left side. The carbon profile depends on both the displacement rate of the moving boundary, i.e., the growth rate of oxide, and the carbon displacement in the opposite direction by diffusion within the RGL.

What are the experimental arguments that support the above hypothesis of mechanism?

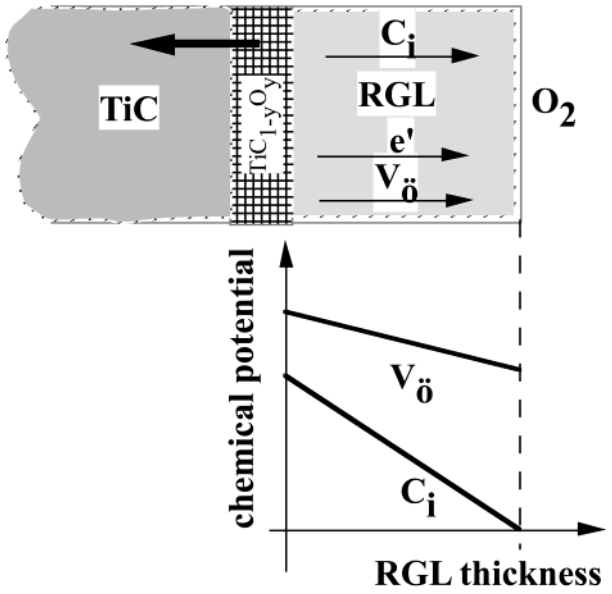

Figure 6. Scheme of the proposed mechanism of the RGL.

(i) The values of the ratio between the O_2 and CO_2 signals (Figure 2) are different from 0.5, as it would be expected in the case of a complete oxidation of both Ti and C of TiC, and they are consistent with the retention of carbon according to the whole reaction

$$TiC + [1 + \alpha - (x/2)]O_2 = TiO_{2-x} + \alpha CO_2 + (1 - \alpha)C \quad (5)$$

where $0 \le \alpha \le 1$. In this case, $\Psi = \alpha/(1 + \alpha - x/2)$ and its value is in the range $0 < \Psi < 1/2$ assuming $x/2$ is negligible with respect to $(1 + \alpha)$. By inspection of Figure 2, the Ψ values are confined for both the samples in the limits expected for a complete combustion: the combustion of C at the RGL/gas interface that diffuses within the RGL and reaction 5. In the former case, $\Psi = 1$.

(ii) The rate of consumption of O_2 is always greater than the absolute value of the rate of production of CO_2 as displayed in Figure 7 (top). This is a proof that the oxidation of Ti and combustion of C are processes with independent kinetics. The curves have been obtained from the first derivative with respect to time of the best fitting curves reported in Figure 2.

(iii) The C profiles along the cross-section of the samples show that they both are characterized by a maximum as found by the micro-Raman scanning, whereas the rutile profiles are always an increasing function reaching a constant value at RGL/gas interface (Figure 4).

(iv) The SEM analysis (Figure 5) shows clearly that the RGL is quite compact and well adherent to the carbide substrate. This supports the feasibility of a solid-state mass-transport, otherwise all the above considerations fall. For both the samples, the SEM analysis showed a lighter compact layer <3 μm thick. This should be attributed to almost pure rutile. From micro-Raman analysis we detected the signal of rutile in a wider range of thicknesses reaching the maximum at the RGL/gas interface. Therefore, we can attribute the bottom darker layer which appears in Figure 5A and B to a region that reacted only partially with the incoming oxygen.

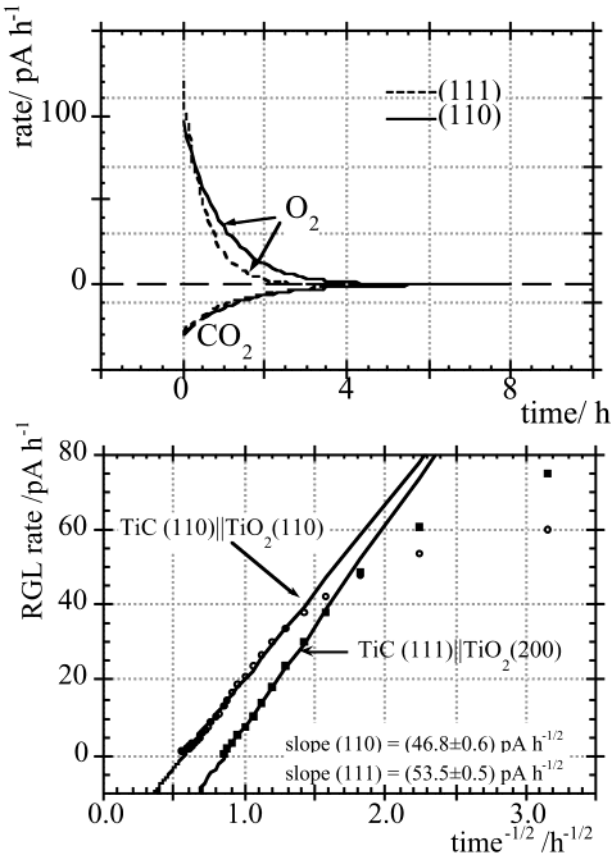

Figure 7. Upper figure: rate of O_2 consumption and CO_2 production obtained by the 1st derivative with respect to time of the best-fitting curves reported in Figure 2. Lower figure: test of the parabolic growth of the RGL: $r_{RGL} = r_{O_2} - |r_{CO_2}|$.

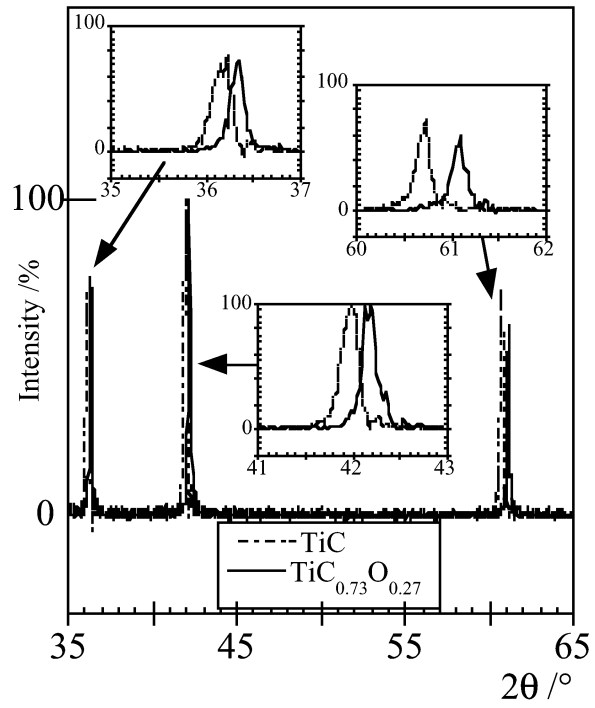

Figure 8. XRD spectra at Cu Kα1 radiation of TiC and $TiC_{0.73}O_{0.27}$ obtained by high-temperature reaction between TiO_2 and TiC powders.

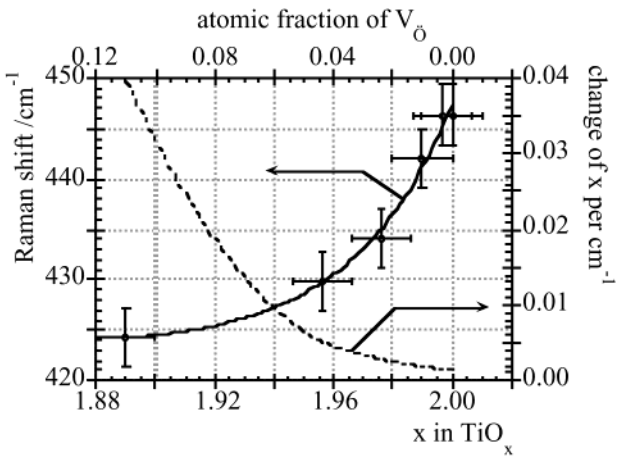

Figure 9. Left ordinate: Raman shift of the rutile peak at 447 cm^{-1} as a function of the oxygen defectivity as given in the literature.[24] Upper abscissa: atomic fraction of oxygen vacancies in rutile. Right ordinate: change of oxygen defectivity per cm^{-1} as obtained by the reciprocal value of the first derivative with respect to x of the best-fitting curve of the experimental Raman shift.

Contrarily to the proposed mechanism, no evidence has been found of any oxycarbide profile nor any changes in the micro-Raman spectra of rutile indicating different x values in TiO_{2-x}.

It is reported in the literature[21] that the substitution of C with O in TiC does not modify its rock salt structure. This is also shown by looking at cell parameters which do not change significantly with respect to the cell parameters of TiC (TiC, a = 432.74 pm;[22] for instance, in $TiC_{0.73}O_{0.27}$, a = 431.2 pm). Therefore, it is expected that oxycarbide also is not Raman active, as it has been checked by us on a synthesized Ti oxycarbide. In fact, we prepared $TiC_{0.73}O_{0.27}$, the XRD spectrum of which is reported in Figure 8, by heating (in high vacuum by electron gun[23]) a stoichiometric mixture of TiC and TiO_2 and the product was examined by micro-Raman. No signal was recorded in the range from 58 to 1750 cm^{-1}.

Several papers[24−26] can be found in the literature on the Raman characterization of the defective oxides of Ti, and particularly of the Magneli phases. In the left ordinate of Figure 9, the data of the displacement of the Raman peak at 447 cm^{-1} vs x in TiO_x, as given in reference 24,[24] are reported. In the right ordinate is shown the calculated curve of the change of x per cm^{-1} as function of x derived from the best fitting of the experimental values. In the upper abscissa, the atomic fraction of the oxygen vacancies, $V_{Ö}$, in rutile is also reported. In the limits of the experimental resolution (±1 cm^{-1}) of the micro-Raman measurements and close to stoichiometric rutile, variations of x within $\approx 4 \times 10^{-3}$ cannot be esteemed. The position of the peak at 447 cm^{-1} was found independent of the distance from the carbide/RGL interface. The constant stoichiometry of rutile throughout the RGL is explained on the basis of the constancy of the free energy of reaction 4. At constant temperature and in steady-state conditions neither the standard free energy nor the activities of

(21) Ouensanga, A. *J. Less-Common Met.* **1979**, *63*, 225.
(22) International Center for Diffraction Data; PCPDFWIN v.2.2, database JCPDS 32-1383.
(23) Latini, A.; Di Pascasio, F.; Gozzi, D. *J. Alloys Compd.* **2002**, *346*, 311.
(24) Parker, J. C.; Siegel, R. W. *Appl. Phys. Lett.* **1990**, *57*, 943.
(25) Turkovic, A.; Ivanda, M.; Vranesa, V.; Drasner, A. *Vacuum* **1992**, *43*, 471.
(26) Parker, J. C.; Siegel, R. W. *J. Mater. Res.* **1990**, *5*, 1246.

oxygen and carbon change. Furthermore, the free energy change of $TiC_{1-y}O_y$ formation also remains unchanged as its stoichiometry is always the same because of the threshold in the $y/(1-y)$ ratio that fixes its upper limit of stability.

The Ψ values for both the samples suggest that TiC oxidation occurs by replacement of C atoms with O atoms. According to this substitution process, we expect the existence of a structural relationship between the TiC substrate and the grown TiO_2 film. Our previous results[11,12] revealed the oriented growth of rutile film on TiC substrates as $TiO_2(200)||TiC(111)$ and $TiO_2(110)||TiC(110)$. The texture measurements showed that TiO_2 grows with the (200) planes exactly on the TiC(111) planes.[12] These data suggest that in the growth of TiO_2 film the positioning of the O atoms replaces the original C sublattice. This agrees with the proposed substitution process where C atoms are replaced by O atoms. The replacement has to be followed by a rearrangement of the TiC structure to turn it from the face centered cubic to the rutile tetragonal structure. Several authors have suggested and/or observed the presence of C in the TiO_2 phase.[6−10] In the present case, it has been possible to observe the C presence by micro-Raman analysis without chemically or mechanically removing the oxidized layer from the bulk sample.

The CO_2 production cannot be explained by the diffusion through the oxide layer because it would lead to a continuous disruption of the oxide film.[8,9] This is in contrast with both the kinetics behavior observed and the adherent TiC/TiO_2 interface as showed by the SEM analysis. Therefore, CO_2 is produced at the RGL/gas interface instead of the TiC/RGL interface. Various authors[6,8−9] have suggested that C diffuses through the rutile layer to be oxidized at the outer surface. On the other hand, outward diffusion of C across the oxide layer may occur only if it were sufficiently soluble therein.[9] Unfortunately no data are available about this.

By inspection of Figures 2 and 7, it appears clearly that the kinetic behavior is not the same for the two samples. According to the structural relationship $TiO_2(200)||TiC(111)$ and $TiO_2(110)||TiC(110)$[12] as well as the proposed mechanism, the different reactivity could be attributed to the anisotropy of the diffusion coefficient of the diffusing species within the RGL and, particularly, $V_{\ddot{O}}$. The tetragonal crystal structure of rutile causes anisotropy in all the physical properties and also in any diffusion process. Consequently, a complete description of the diffusion of any species in the rutile structure requires two principal diffusion coefficients, one parallel, $D_{||}$, and one perpendicular, $D_{\perp}$, to the *z*-axis. To this purpose, the *c* axis is oriented such that it coincides with the *z*-axis of a Cartesian coordinate system. The diffusion coefficient *D* in any direction with the angle φ between the diffusion direction and the *z*-axis, is then given by relation: $D = D_{||}\cos^2\varphi + D_{\perp}\sin^2\varphi$. Experiments reported in the literature[27−29] with rutile single crystals showed a faster diffusion along the *a*-axis in contrast to the high interstitial mobility along the *c*-axis of metal impurities. For $V_{\ddot{O}}$, the ratio $D_{||}/D_{\perp} = 1.6$. This different behavior is probably due to the shorter O−O distances (0.252 vs 0.296 nm) along the *a*-axis, because considering the large size of the oxygen ion, fast diffusion through the channels of the *c*-axis would not be expected.

According to the above evidence, the reactivity of TiC(111) should be higher because the (200) planes of rutile are orthogonal to the *a*-axis whereas (110) planes are at 45° with respect to it. All this concerns the pure diffusion process in rutile, whereas in the present case we are dealing with a more complex process involving oxygen: solid-state reaction, i.e., reaction 4, preceded by diffusion of oxygen vacancies $V_{\ddot{o}}$ and followed by nucleation and growth of RGL. The results reported in Figure 7 (top) show that the rate of O_2 consumption depends on the RGL orientation contrarily to the diffusion of C, i.e., the rate of formation of CO_2. To test the parabolic growth of the RGL, the growth rate of RGL, r_{RGL}, has been plotted vs $t^{-1/2}$ in Figure 7 (bottom). The RGL growth rate is given by $r_{RGL} = r_{O_2} - |r_{CO_2}|$ being r_{O_2} and r_{CO_2}, respectively, the rate of the *total* oxygen consumed, and CO_2 production. Thus, the r_{RGL} is the rate to which oxygen is consumed only for the RGL growth. According to the law of parabolic growth,[30] the square of the RGL thickness should be proportional to time through the parabolic rate constant. In the present case, other constant terms are embedded in the proportionality constant which are unknown (though they are equal in both the experiments on the two single crystal samples). Therefore, the comparison between the slopes of the straight lines reported in Figure 7 (bottom) is self-consistent and their values depend only of the respective parabolic constants. It appears that the surface (111) of TiC, upon which the RGL grows (200) oriented, is kinetically favored below the estimated error. Looking at Figure 1, where an independent measurement with respect to the QMS measurement was performed by oxygen sensors, the rate of oxygen consumed is displayed. This quantity is the rate of total oxygen, i.e., r_{O_2}. It appears clearly that $r_{O_2}(110) > r_{O_2}(111)$ in agreement with the QMS data reported in Figure 7 (top). It is important to point out the conceptual difference between oxygen measured both by oxygen sensors and QMS, which is the quantity $[1 + \alpha - (x/2)]$ in reaction 5, and oxygen for growing the RGL equal to $[1 - (x/2)]$. Therefore, though $r_{O_2}(110) > r_{O_2}(111)$, $r_{RGL}(110) < r_{RGL}(111)$. This would imply that the rate of diffusion of carbon in the RGL (110) oriented is greater than the rate of diffusion in the RGL (200) oriented. These results confirm our previous findings[12] which were obtained through a rough estimation of α, because at that time the QMS measurements were not available.

The diffusion of C through the RGL controls the rate of its combustion reaction at the RGL/gas interface. Data of diffusion of C in rutile are unknown, though it is expected its diffusion mechanism would exhibit a behavior similar to that of $V_{\ddot{O}}$.

The trend of Ψ reported for both the samples in Figure 2 is quite different, and, in the case of TiC(111), Ψ passes through a maximum the value of which is close to 1, i.e., oxygen is consumed almost entirely for carbon

(27) Blumenthal, R. N.; Baukus, J.; Hirthe, W. M. *J. Electrochem. Soc.* **1967**, *114*, 172.
(28) Gruenwald, T. B.; Gordon G. *J. Inorg. Nucl. Chem.* **1971**, *33*, 1151.
(29) Haul, R.; Dümbgen, G. *J. Phys. Chem. Solids* **1965**, *26*, 1.
(30) Kofstad, P. *High-Temperature Corrosion*; Elsevier Applied Science: London, 1988.

combustion. Such evidence shows that at a certain stage of evolution of RGL, reaction 4 is practically stopped, and the combustion of C arriving at the RGL/gas interface remains the unique process to consume oxygen. In the case of TiC(110), the whole trend of Ψ follows the expected behavior: increasing the thickness of RGL, its growth rate tends to zero because the flux of oxygen vacancies vanishes, so Ψ increases, whereas interstitial carbon continues to diffuse practically with the same flux because its chemical potential gradient does not change significantly.

5. Conclusions

Through the results presented in this work some new information enters into the knowledge of growth kinetics of oxide films when transition metal carbides are exposed at high temperatures to gaseous atmospheres at controlled fugacity of oxygen. The experiments performed are in part in situ experiments − oxygen sensors and QMS measurements − that give the real-time kinetics concerning the O_2 consumption and CO_2 production. On the other hand, they do not display clear-cut evidence of what really occurs at the interfaces or in the bulk of the rutile film. At the present stage, to propose a growth model consistent with on-line and off-line experimental evidence, we proceeded by assuming reasonable working hypotheses that will require more sophisticated experiments, such as in situ synchrotron radiation spectroscopies, to be definitively proven.

Acknowledgment. This work was partially financed by the ISMN of the National Research Council. We are indebted to S. Shimada of Hokkaido University, Sapporo, for supplying samples of TiC single crystals. The cooperation of S. Loreti and C. Minarini of the ENEA research laboratories, respectively, in Frascati (Rome) and Portici (Naples), for x-ray texture analysis is gratefully acknowledged. The invaluable cooperation given by P. L. Cignini of ISMN for his contribution to the experimental work is also gratefully acknowledged.

CM021204C